Piotr LESIAK
TECHNICAL UNIVERSITY IN RADOM, FACULTY OF TRANSPORT

Accuracy of automated ultrasonic measurements of rail track defects – selected issues

Piotr LESIAK, M.Sc., Ph.D.

Graduate of Gdańsk University of Technology Electrical Engineering Faculty. Ph.D. thesis defended with honours in 1980 – Faculty of Electrical Engineering of Warsaw University of Technology. Since 1973 works at Radom Univeristy of Technology. During 10 last years head of Transport Automation and Telematics Institute. His scientific and educational interests include investigation and design of measurement and diagnostics devices for rail transport and measurement systems. Three times MEN prize winner for scientific achievements.

e-mail: p.lesiak@pr.radom.pl

Abstract

On the basis of automated flaw detection of rails, the basic dependencies describing localisation and dimensions of object's inner defects traced with ultrasonic pulse-echo method have been given in the paper. The formulas for systematic errors and limiting errors estimating measurement accuracy have been determined. The investigation has been illustrated with results obtained by numerical simulation and with experimental test results acquired from flaw detection vehicle track testing.

Keywords: measurement errors, ultrasonic flaw detection, railway rail.

Dokładność zautomatyzowanych pomiarów wad w szynach kolejowych metodą ultradźwiękową – wybrane zagadnienia

Streszczenie

Podano podstawowe zależności opisujące położenie i wymiary wewnętrznych wad obiektu badanych ultradźwiękową metodą echa na przykładzie zautomatyzowanej defektoskopii szyn kolejowych. Wyznaczono wzory dla błędów systematycznych i błędów granicznych jako miar dokładności tych pomiarów. Rozważania poparto wynikami otrzymanymi z symulacji komputerowej oraz z badań toru kolejowego wagonem pomiarowym.

Słowa kluczowe: błędy pomiarowe, defektoskopia ultradźwiękowa, szyna kolejowa.

1. Introduction

The technical condition assessment of rails in the railway track is based on the automated flaw detection testing. Specialised equipment including ultrasonic devices is used in the tests. The equipment is placed either in flaw detection vehicle or in the go-devil [2, 4 and 6]. The position and contours of inner flaws are determined with the help of integrated probe sets, which are moved along the rail head surface. The obtained results should be credible, since they are used to classify the defects.

Therefore it is necessary to assess the accuracy of parameters measured by the equipment, in particular in case of values verging on the critical. If the flaw is classified as hazardous, then the rail section must be replaced. Wrong classification or non-detection of flaw may cause huge economic losses and expose people to danger. Lesser flaws are subjected to further monitoring.

The accuracy of manual ultrasonic measurements by pulse-echo method has been discussed in [1]. However, lots of important issues related to test automation have not been considered. Analysis of flaw imaging accuracy in railway rails has been given in [3].

This paper gives the outline of accuracy of flaw location and size determination in railway rails. For reasons related to flaw dimension classification results, the limiting errors were adopted as test results accuracy measures. The discussion is supplemented by computer simulation and experimental railway track tests results.

2. Measurement principle - basic dependencies

During automated rail measurements, ultrasonic probe moves along the rail head at V velocity. Owing to good acoustic coupling (continuous water bath), the probe emits ultrasonic wave beam into the rail at ΔT_e time period. Wave emission frequency $1/\Delta T_e$ is directly proportional to probe movement velocity V, so that it occurs at constant intervals ΔX, e.g. every 2,5, or 10 mm, which constitute single scanning mesh length - see fig. 1a.

In case of angular probe, the transverse wave T propagates inside the rail at C_T velocity and in direction β – fig. 1a; after being reflected from the flaw it partially comes back to the head. To analyse measurement accuracy, it is necessary to be familiar with formulas related to measurements. This is equivalent to solving a planar 2D image in vertical rail cross-section along the probe head movement path. Rail height is measured with maximum 8-bit resolution, which determines mesh height ΔY. For instance, in case of S49-type rail with approximate height 150 mm, the mesh height is calculated as $\Delta Y \approx 0.6$ mm. The mesh height is closely related to wave beam passage time in the mesh ΔT, since $\Delta Y = C_T\, \Delta T \cos\beta$. If the vertical resolution is diminished, when $\Delta X = \Delta Y\, tg\beta$, then wave beam axis is parallel to mesh diagonal [2].

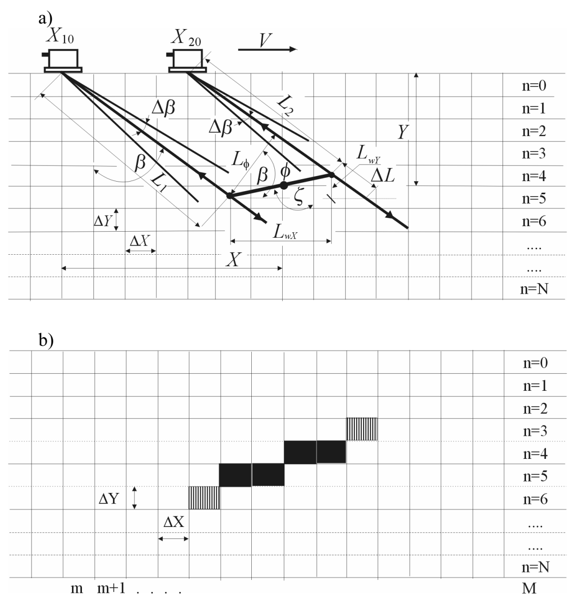

Fig. 1. a) Ultrasonic testing of inner flaw Φ mm long b) flaw's discretised image

The local co-ordinates X,Y of the flaw's position are determined in relation to the probe position X_m at the time instant, when the wave is being emitted. For the point reflecting the beam axis the following geometrical dependencies are true:

$$X = L_n \sin\beta = 0{,}5\ C_T\left(t_n^{'} - t_g\right)\sin\beta \tag{1a}$$

$$Y = L_n \cos\beta = 0.5\, C_T\left(t_n^{'} - t_g\right)\cos\beta \tag{1b}$$

where: $t_n^{'} = t_n + t_g$ – total return time of the reflected beam (beam travelling towards probe transducer), $t_n = \dfrac{2L_n}{C_T}$, $t_g = \dfrac{2L_g}{C_L}$ – wave passage time – within the rail and the probe, respectively L_n, L_g - wave path lengths in the rail and the probe, C_L – longitudinal wave L velocity in the probe.

When the measurements are discretised within Y axis, then in accordance with (1a,b) it is seen that the local co-ordinates of the mid-mesh point at nth level are equal to:

$$X_n = 0{,}5\, C_T\, t_n \sin\beta \approx (n+0{,}5)\Delta Y\, tg\beta \tag{2a}$$

and

$$Y_n = 0{,}5\, C_T\, t_n \cos\beta \approx (n+0{,}5)\Delta Y \tag{2b}$$

where: $t_n \approx \dfrac{(2n+1)\Delta Y}{C_T \cos\beta}$.

The ultrasonic wave beam running through the rail is divergent. The divergence of beam cross-section in the far-field is determined by $2\Delta\beta$ angle – see fig. 1a. This angle depends on the probe transducer diameter D and wave frequency f and adopted coefficient k_u, related to relative amplitude drop in the direction transverse to β axis (e.g. for 6 dB, $k_u = 0{,}5$) and wave velocity C_T, i.e.

$$\Delta\beta = \arcsin\frac{k_u C_T}{f\, D} \tag{3}$$

Wave amplitude becomes diminished along wave's path, due to damping and dissipation. In order to obtain return wave signals independent of flaw depth, automatic correction is used, achieved by so-called distance gain control. The formulas describing flaw dimensions are simplified, if wave return times are measured for amplitude with drop coefficient $k_u = 0.5$. Then it may be assumed and with sufficient accuracy too, that flaw dimensions may be determined by wave beams measurements, for beam axes running through flaw contours as seen from β direction – fig. 1a. This greatly simplifies geometrical formulas, since it is not necessary to consider the influence of beam divergence angle $\Delta\beta$ and its variations.

The flaw's edges co-ordinates can be calculated from simple geometric formulas:

$$X_{w1} = X_{10} + L_1 \sin\beta\,,\;\; X_{w2} = X_{20} + L_2 \sin\beta \tag{4a}$$

$$Y_{w1} = L_1 \cos\beta\,,\;\; Y_{w2} = L_2 \cos\beta \tag{4b}$$

where: X_{10}, X_{20} – actual co-ordinates of probe centre during flaw edges measurements, $L_1 = C_T t_1$, $L_2 = C_T t_2$ – the beam path lengths from the probe to both flaw edges, determined by measuring t_1, t_2 time intervals with flaw detector.

The difference of rectangular co-ordinates of flaw edges is called flaw spread and for a discretised two beams path difference $\Delta L = L_1\text{-}L_2 \approx \dfrac{\Delta n\, \Delta Y}{\cos\beta}$ it is equal to, respectively:

$$L_{wX} = X_{20} - X_{10} - \Delta L \sin\beta = \Delta m \Delta X - \Delta n \Delta Y\, tg\beta\,,\;\; L_{wY} = \Delta n\, \Delta Y \tag{5a,b}$$

The flaw length Φ and the angle of inclination of the segment joining its edges ζ may be derived from (5a,b):

$$\Phi = \sqrt{L_{wX}^2 + L_{wY}^2} = \sqrt{(\Delta m\, \Delta X)^2 - 2\,\Delta m\, \Delta X\, \Delta n \Delta Y\, tg\beta + \frac{(\Delta n \Delta Y)^2}{\cos^2\beta}} \tag{6a}$$

$$\xi = arc\,tg\frac{L_{wX}}{L_{wY}} = arc\,tg\left(\frac{\Delta m\, \Delta X}{\Delta n\, \Delta Y} - tg\beta\right) \tag{6b}$$

At the same time, the probe „sees" a flaw image with equivalent length $L_\Phi = (X_{20} - X_{10})\cos\beta = \Phi \sin(\beta + \xi)$, perpendicular to propagation direction β (fig. 1a).

In measurement practice the spread of flaw is measured. It is reconstructed on the basis of signals with amplitude greater than the comparison level set in the measurement device.

The meshes which have been eliminated from the reconstructed flaw image in accordance with the above method, at amplitude drop coefficient $k_u = 0.5$, are marked in fig.1b with lighter colour.

3. Discretised flaw measurements accuracy

The X and Y co-ordinates of beam reflection point are determined locally, i.e. in relation to actual probe position at the emission time instant. They are calculated from formula (1a, b) on the basis of total wave return time t'_n measurement. If the time t_g (equal to beam propagation time in the probe) is not subtracted, then the results are excessive; in other words, error of method occurs, with absolute values for both co-ordinates equal to, respectively:

$$\Delta_X = 0{,}5\, C_T t_g \sin\beta\,,\;\; \Delta_Y = 0{,}5\, C_T t_g \cos\beta \tag{7}$$

The relative error of method for both co-ordinates is the same, or:

$$\delta_X = \delta_Y = \frac{t_g}{t_n} \tag{7a}$$

The error is eliminated during measurement device calibration, and therefore need not be taken into account.

If the flaw spread in the X direction is calculated approximately only as a difference of the probe positions $X_{m+1,0}$-$X_{m,0}$, where the flaw edges are investigated, then the error of method is equal to:

$$\Delta_{Lx} = C_T\left(t_1 - t_2\right)\sin\beta \tag{8}$$

Measurement accuracy under nominal conditions is described with **basic errors**. For the local point co-ordinates X, Y they are derived from total differential of formulas (1a, b), for flaw edges seen in β direction - from (4a, b) differential, and for equivalent dimensions – from (5) and (6a).

The relative errors of flaw location related to actual values of both local co-ordinates X, Y are equal to:

$$\delta_X = \delta_{C_T} + \frac{1}{t_n}\Delta_{t_n} + \Delta_\beta\, ctg\beta\,,\;\; \delta_Y = \delta_{C_T} + \frac{1}{t_n}\Delta_{t_n} - \Delta_\beta\, tg\beta \tag{9}$$

Additional errors arise, when there is a discrepancy between inner rail parameters and device parameters and nominal measurement conditions. With rails flaw detection, these parameters are L_g (wave path length), C_L (wave velocity in the probe) and C_T (wave velocity in the rail).

Using Snell's law expressed as $\sin\beta = \dfrac{C_T}{C_L}\sin\alpha$ and assuming that probe wedge α = const, for wave velocity relative errors δ_{C_T}, δ_{C_L} the following change in β angle is obtained:

$$\Delta_\beta = \left(\delta_{C_T} - \delta_{C_L}\right) tg\beta \tag{10}$$

where: δ_{C_L} - error for forecasted maximum temperature rise in the Plexiglas probe wedge (*c.* 20^0 C- continuous water cooling), it is equal to *c.* 2%, δ_{C_T} - error depends mostly on acoustic properties of the material and its homogeneity (e.g. in case of rails, depending on the type of steel the variation is *c.* ±200 m/s, in particular in welded joints). The impact of temperature is about 10 times less than for the probe casing.

Then, it is obtained from (9):

$$\Delta_X = Y\left[2\delta_{C_T} - \left(1 + \frac{t_g}{t_n}\right)\delta_{C_L} + \frac{1}{t_n}\Delta_t - \frac{t_g}{t_n}\delta_{Lg}\right] \tag{11a}$$

$$\Delta_Y = Y\left[\left(1 - tg^2\beta\right)\delta_{C_T} + \frac{1}{t_n}\Delta_t + (tg^2\beta - \frac{t_g}{t_n})\,\delta_{C_L} - \frac{t_g}{t_n}\delta_{Lg}\right] \quad (11b)$$

where: $Y = 0{,}5 C_T t_n \cos\beta$, Δ_t – time measurement absolute error (for the flaw detector used this error was equal to $0{,}133.10^{-6}$ s), δ_{Lg} - relative dispersion error for wave path in the probe; e.g. if the probe wear is 1 mm, then for T70 head (path length in the wedge being equal to *c.* 15 mm) the error was *c.* 7%, and for T45 head (path length in the wedge being equal to *c.* 10 mm) the error was *c.* 10%.

When discretisation is taken into account, then the absolute limiting errors are calculated on the basis of (11a and b):

$$\left|\Delta_{Xn}\right|_{gr} = \left|(2n+1)\,\Delta Y\right|\left|\delta_{C_T}\right| + \left|\left[(n+0{,}5)\Delta Y + 0{,}5\frac{C_T L_g\cos\beta}{C_L}\right]\right|\left|\delta_{C_L}\right| + \left|(C_T\cos\beta)\right|\left|(\Delta_t + \Delta T)\right| + \left|0{,}5\frac{C_T L_g\cos\beta}{C_L}\right|\left|\delta_{Lg}\right| + \left|\Delta X\right| \quad (12a)$$

$$\left|\Delta_{Yn}\right|_{gr} = \left|(n+0{,}5)\Delta Y\left(1 - tg^2\beta\right)\right|\left|\delta_{C_T}\right| + \left|\left[(n+0{,}5)\Delta Y tg^2\beta - 0{,}5\frac{C_T L_g\cos\beta}{C_L}\right]\right|\left|\delta_{C_L}\right| + \left|(C_T\cos\beta)\right|\left|(\Delta_t + \Delta T)\right| + \left|0{,}5\frac{C_T L_g\cos\beta}{C_L}\right|\left|\delta_{Lg}\right| + \left|\Delta Y\right| \quad (12b)$$

and both relative errors $\left|\delta_{Xn}\right|_{gr}$, $\left|\delta_{Yn}\right|_{gr}$, related to flaw mesh position (2a and b), respectively. They can also be related to the measurement range or rail height.

In a similar way, absolute errors L_{wX}, L_{wY} of flaw spread dimensions can be obtained:

$$\Delta_{LwX} = \Delta_{(X_{20} - X_{10})} - \Delta L\left(2\delta_{C_T} - \delta_{C_L}\right)\sin\beta - C_T\Delta_{(t1-t2)}\sin\beta \quad (13a)$$

$$\Delta_{LwY} = \Delta L\cos\beta\left[\delta_{C_T}\left(1 - tg^2\beta\right) + \delta_{C_L}\ tg^2\beta\right] + C_T\Delta_{(t1-t2)}\cos\beta \quad (13b)$$

If discretisation is used, then limiting errors will be equal to:

$$\left|\Delta_{LwX}\right|_{gr} = \Delta m\left|\Delta_{\Delta X}\right| + \Delta X + \Delta n\,\Delta Y\left(2\left|\delta_{C_T}\right| + \left|\delta_{C_L}\right|\right)tg\beta + C_T\sin\beta\left|\Delta_{(t1-t2)}\right| + \left|\Delta Y\right|tg\beta \quad (14a)$$

$$\left|\Delta_{LwY}\right|_{gr} = \Delta Y\left[\Delta n\left(\left|1 - tg^2\beta\right|\left|\delta_{C_T}\right| + \left|\delta_{C_L}\right| tg^2\beta\right) + C_T\left|\Delta_{(t1-t2)}\right|\cos\beta + 1\right] \quad (14b)$$

where: $\left|\Delta_{(t1-t2)}\right| = \left|\Delta_{t1}\right| + \left|\Delta_{t2}\right| = 2\left|\Delta_t\right|$, $\Delta_{\Delta X}$ - absolute error of probe path along the rail, measured with encoder. For a railway track this error averages 1 m per 1 km.

4. Simulation tests of limiting errors

Figs. 2 - 4 show simulation tests results of flaw measurements limiting errors. The tendency of flaw position error increase corresponding to increase in probe angle may be observed – figs. 2a, b and 3b. Since the quantisation error is present, all types of errors attain maximum values for initial mesh levels – fig. 3a. In practice, another limitation of tests conducted away from the rolling surface of rail head with single transducer probes is transducer's dead zone. That is why satisfactory results are usually obtained above ten or more millimetres (during simulations it was assumed that $n \geq 25$).

The impact of wave velocity C_T is insignificant - fig. 3a and b, therefore its dependence on temperature can be neglected during rail service tests.

If we must assess, whether the flaw is dangerous, then limiting error of the flaw spread are significant – figs. 4a and b.

Moreover, fig. 5 presents values of flaw spread measurement limiting errors, flaw located at $n = 20$ level, probe angle $\beta = 70$ at wave velocity $C_T = 3200$ m/s and a set number of probe steps Δm. When $\Delta m = 4$ (fig. 4b), the limiting error of the flaw height is 23 mm, and when Δm increases, this error also increases. The reason for this effect is diminishing flaw inclination angle ξ, which leads to flaw's reduced emission capacity. In particular, using probes with bigger angles is unfavourable, since the planar path of the wave beam in the rail leads to increase in flaw envelope (fig. 4b).

Two other examples of flaw spread limiting errors are shown as a matrix in fig. 6. They have been obtained for typical measurement probes. The limits increase, as distance n grows. For instance, in case of 12 mm high flaw, tested with a probe $\beta = 70$, the length increase will be 21 mm, or at least two meshes along the rail. This may significantly change flaw classification. The assumed flaw length does not matter here, as opposed to its height and probe angle – this can also be seen from fig. 4a.

a)

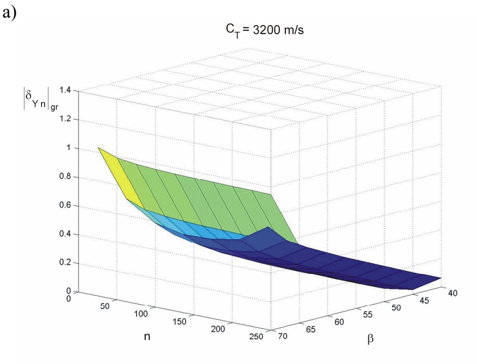

b)

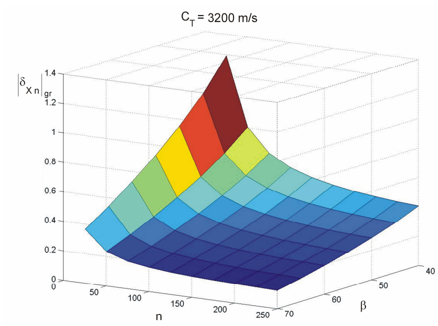

Fig. 2. Relative limiting errors calculated for flaw position n, a) depth of the flaw, b) position of the flaw along the rail - vs. probe angle β and level number n

a)

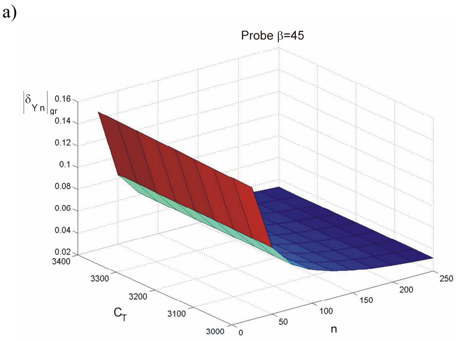

b)

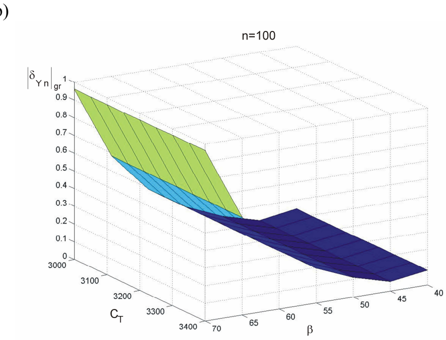

Fig. 3. Relative limiting errors of flaw depth vs. wave velocity in the rail C_T and a) level number n, b) probe angle β

a)

b)

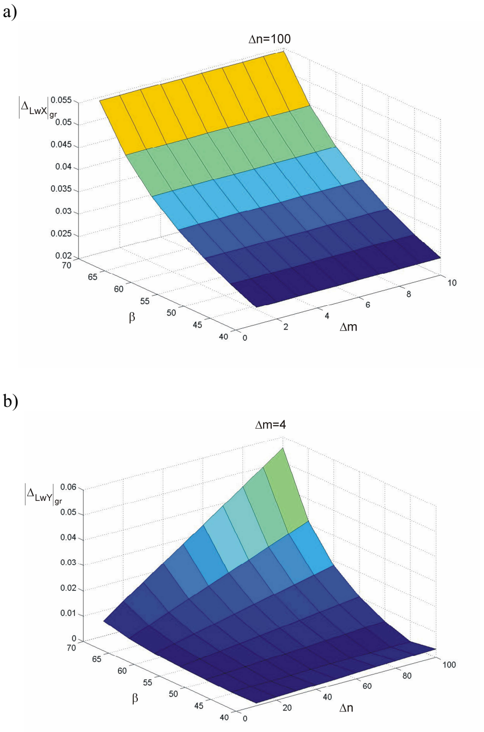

Fig. 4. Absolute error of the flaw spread vs. probe angle β and a) step increase Δm of the probe along the rail at a given flaw height equal to Δn = 100 meshes, and as a function of b) flaw height Δn at a constant probe step increment Δm = 4

$$\Delta n=20,\ \beta=70 \qquad \left|\Delta_{LwY}\right|_{gr}=\begin{bmatrix}0.006\\0.012\\0.017\\0.023\\ \cdot\\ \cdot\\0.055\end{bmatrix}\begin{array}{c}\Delta m=1\\2\\ \cdot\\4\\ \cdot\\ \cdot\\10\end{array} \qquad \Delta n=20,\ \Delta m=4 \qquad \left|\Delta_{LwY}\right|_{gr}=\begin{bmatrix}0.001\\0.002\\ \cdot\\ \cdot\\ \cdot\\0.013\\0.023\end{bmatrix}\begin{array}{c}\beta=45\\ \beta=50\\ \cdot\\ \cdot\\ \cdot\\ \beta=65\\ \beta=70\end{array}$$

Fig. 5. Flaw height spread limiting errors matrix

$$\beta=70 \qquad \left|\Delta_{LwX}\right|_{gr}=\begin{bmatrix}0.021\\0.029\\0.038\\0.046\\0.054\end{bmatrix}\begin{array}{c}\Delta n=20\\40\\ \cdot\\ \cdot\\100\end{array} \qquad \beta=45 \qquad \left|\Delta_{LwX}\right|_{gr}=\begin{bmatrix}0.014\\0.017\\0.020\\0.024\\0.027\end{bmatrix}\begin{array}{c}\Delta n=20\\40\\ \cdot\\ \cdot\\100\end{array}$$

Fig. 6. Examples of flaw height spread limiting errors matrices

A significant improvement can be achieved by scan mesh condensing dependent on flaw detection vehicle speed – a software procedure used in novel measurement devices employed by PKP [4].

5. Railway track measurements – examples

Measurement window of the rail flaw detection vehicle software is shown in fig. 7. Using the probe with angle $\beta = 45$ and emission every ΔX = 5mm, a flaw in the S60 type rail has been detected (location 23,773 km at one railway track). The following spreads have been obtained: length L_{wX} = 35mm ($\Delta m = 7$), height L_{wY} = 10mm ($\Delta n \cong 15$) and flaw depth (location) Y_n = 115mm (level n = 173 at $\Delta Y \approx 0.66$ mm). Without analysing measurement error this flaw has been classified as one to be monitored (mark „O" at fig. 7). The limiting errors here are equal to, respectively: $\left|\Delta_{Yn}\right|_{gr}$ = 4,8mm ($n \cong 7$), $\left|\Delta_{LwX}\right|_{gr}$ = 9,3mm ($\Delta m \cong 2$), $\left|\Delta_{LwY}\right|_{gr}$ = 0,9mm ($\Delta n \cong 2$). These errors may constitute the basis for a change in classification – flaw may be graded as hazardous (mark „W"; this type of flaw has also been recorded in the measurement window – see fig. 7), since the external allowable dimensions have been exceeded, when the limiting error has been added to the measured length value.

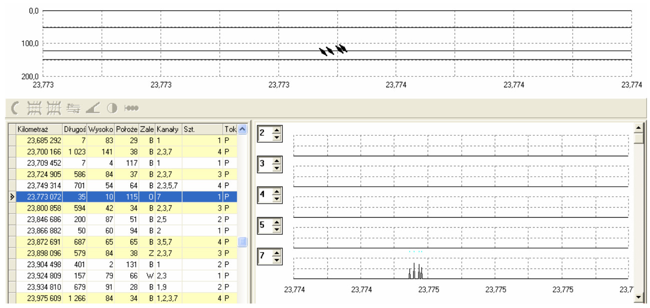

Fig. 7. Example of flaw measurement recording (railway track)

6. Conclusions

Analysis of given formulas, simulation tests and experimental tests conducted so far shows that, while assessing the dimensions of inner discontinuities of railway rails, tested by ultrasonic pulse-echo methods, it is absolutely indispensable to take into account measurement accuracy. This may be achieved by working out the limiting error matrices for different probes used in flaw detection vehicle and using them in automated tests to assess measurement results. In particular, the flaw spread errors leading to improper flaw classification (hazardous or non-hazardous) are very important. Flaw depth errors may lead to the change in flaw type assessment according to UIC classification [5]. The errors of flaw location along the rail are significant only in the case when the flaw image is constructed by superimposing measurements taken from several probes, since the flaw total spread might then be increased.

A more complete picture of reliability and accuracy of conducted measurements may be obtained, if the statistics of random errors occurring in practice in given measurement cycles and under specified conditions are taken into account.

The author wishes to express his gratitude to doc. Zygmunt Warsza for his valuable advice.

7. References

[1] Skorupa A.: Wybrane zagadnienia interpretacji wyników ultradźwiękowych badań czołowych połączeń spawanych. Elektryfikacja i Mechanizacja Górnictwa i Hutnictwa, Zeszyty Naukowe AGH, nr 57 Kraków 1974.

[2] Lesiak P.: System for Automatic Ultrasonic Quality Control of Railroad Rails, Russian Journal of Nonde-structive Testing, Vol. 28:7, 1992.

[3] Lesiak P., Wieczorek D., Malinowski J.: Badania symulacyjne błędów zobrazowania wad w zautomatyzowanej kontroli szyn kolejowych. Materiały XXIV Krajowej Konferencji Badań Nieniszczących, Poznań-Kiekrz 1995.

[4] Lesiak P., Gołąbek P., Ciszewski T., Wieczorek D., Bojarczak P., Korneta A., Rojek B.: Nowa inteligentna aparatura ultradźwiękowa do badania szyn w torze. Zeszyty Problemowe, Badania Nieniszczące, Zeszyt nr 5 z XXIX Krajowej Konferencji Badań Nieniszczących w Krynicy, Warszawa 2000.

[5] Heyder R.: Nowy katalog UIC uszkodzeń szyn. Technika Transportu Szynowego, nr 1–2, 2002, (na podstawie The new UIC of rail defects. Der Eisenbahningenieur 9, 2001).

[6] Lesiak P.: Virtual Instruments and Measurement: Diagnostic Systems in Railway Transportation. Part 1. Ultrasonic Diagnostics for Railway Rails. The Archives of Transport, Vol. XVIII, No 1, 2006.

Artykuł recenzowany